Remote Sensing of Environment 134 (2013) 392–402

Contents lists available at SciVerse ScienceDirect

Remote Sensing of Environment

journal homepage: www.elsevier.com/locate/rse

Mapping deciduous rubber plantations through integration of PALSAR and multi-temporal Landsat imagery

Jinwei Dong [a], Xiangming Xiao [a,*], Bangqian Chen [b], Nathan Torbick [c], Cui Jin [a], Geli Zhang [d], Chandrashekhar Biradar [a]

[a] Department of Microbiology and Plant Biology, and Center for Spatial Analysis, University of Oklahoma, Norman, OK 73019, USA
[b] Rubber Research Institute, Chinese Academy of Tropical Agricultural Sciences, Danzhou, Hainan, 571737, China
[c] Applied Geosolutions, Durham, NH, 03857, USA
[d] Institute of Geographic Sciences and Natural Resources Research, Chinese Academy of Sciences, Beijing, 100101, China

ARTICLE INFO

Article history:
Received 20 November 2012
Received in revised form 1 March 2013
Accepted 18 March 2013
Available online xxxx

Keywords:
Rubber (*Hevea brasiliensis*) plantation
Phenology
Hainan Island
Landsat
PALSAR
Field Photo Library

ABSTRACT

Due to increasing global demand for natural rubber products, rubber (*Hevea brasiliensis*) plantation expansion has occurred in many regions where it was originally considered unsuitable. However, accurate maps of rubber plantations are not available, which substantially constrain our understanding of the environmental and socioeconomic impacts of rubber plantation expansion. In this study we developed a simple algorithm for accurate mapping of rubber plantations in northern tropical regions, by combining a forest map derived from microwave data and unique phenological characteristics of rubber trees observed from multi-temporal Landsat imagery. Phenology of rubber trees and natural evergreen forests in Hainan Island, China, was evaluated using eighteen Landsat TM/ETM+ images between 2007 and 2012. Temporal profiles of the Normalized Difference Vegetation Index (NDVI), Enhanced Vegetation Index (EVI), Land Surface Water Index (LSWI), and near-infrared (NIR) reflectance for rubber trees and natural forest were constructed. The results showed that rubber plantations are distinguishable from natural evergreen forests in two phenological phases: 1) during the defoliation (leaf-off) phase in late February–March, vegetation index (NDVI, EVI, LSWI) values were lower in rubber plantations than in natural evergreen forests; and 2) during the foliation (new leaf emergence) phase in late March–April, rubber plantations had similar NDVI and LSWI values but higher EVI and NIR reflectance values than in natural forests. Therefore, it is possible to delineate rubber plantations within forested landscapes using one to two optical images acquired in the defoliation and/or foliation period. The mapping technique was developed and applied in the Danzhou Region of Hainan. Phased Array type L-band Synthetic Aperture Radar (PALSAR) 50-m Orthorectified Mosaic images were used to generate a forest cover map and further integrated with the phenological information of rubber plantations extracted from Landsat TM images during the foliation phase. The resultant map of rubber plantations has high accuracy (both producer's and user's accuracy is 96%). This simple and integrated algorithm has the potential to improve mapping of rubber plantations at the regional scale. This study also shows the value of time series Landsat images and emphasizes imagery selection at appropriate phenological phase for land cover classification, especially for delineating deciduous vegetation.

1. Introduction

Plantation development by the agroforestry industry, such as the expansion of Pará rubber tree (*Hevea brasiliensis*) plantations, has been a critical driver of land cover change around the world, particularly in the tropics. The Food and Agriculture Organization (FAO) of the United Nations Global Forest Resources Assessment (FRA) 2010 reported that globally rubber plantation extent has steadily increased by 25% during the past two decades (FAO, 2010). Approximately 97% of global natural rubber supply comes from Southeast Asia (Li & Fox, 2012). This land use is a primary driving factor for the conversion from swidden to monocultural cash plantations in montane areas of mainland Southeast Asia (Fox & Vogler, 2005). This land use change process has both economic and environmental outcomes. On the one hand, local farmers can improve financial stability as rubber plantations provide greater agricultural profit due to the increased demand for rubber products. Further, rubber plantations tend to have greater agricultural resiliency compared to traditional cash crops that are more stressed by adverse weather. On the other hand, the

* Corresponding author at: Department of Microbiology and Plant Biology, and Center for Spatial Analysis, University of Oklahoma, 101 David L. Boren Blvd. Norman, OK 73019, USA. Tel.: +1 405 325 8941.
E-mail address: xiangming.xiao@ou.edu (X. Xiao).

0034-4257/$ – see front matter © 2013 Elsevier Inc. All rights reserved.
http://dx.doi.org/10.1016/j.rse.2013.03.014

expansion of rubber plantations plays an important role in altering regional environments that substantially affect human well-being and ecosystem services. For example, large-scale land surface change affects climate, carbon stocks, and biodiversity (Foley et al., 2005; Li, Aide et al., 2007; Ziegler, Fox, & Xu, 2009). Rapid expansion of rubber plantations has occurred in south China due to the increasing demand for rubber products. The rapid growth of rubber plantations in Hainan Province and the Xishuangbanna Region of Yunnan Province in China has received much attention (Qiu, 2009; Zhai et al., 2012; Ziegler et al., 2009); however, an accurate map of rubber plantation extent with high accuracy and resolution is still not available in these regions.

A number of studies have used optical remote sensing data to delineate rubber plantations and these studies can be categorized into two broad groups. The first group focuses on the use of spectral signatures with cluster analysis and traditional classifiers to identify and map rubber plantations. For example, Li et al. (Li, 2011; Li & Fox, 2011, 2012) applied Mahalanobis typicality method to identify rubber trees in mainland Southeast Asia by using spectral data from Moderate Resolution Imaging Spectroradiometer (MODIS), Advanced Spaceborne Thermal Emission and Reflection Radiometer (ASTER), and Landsat imagery. Zhang et al. (2010) used georeferenced field data and Landsat TM images in May-August of 2008 to conduct a maximum likelihood supervised classification that achieved an overall accuracy of 91% in Hainan Island, China, and the rubber plantation area was estimated at 4170 km^2. However, rubber trees have similar spectral characteristics compared to natural tropical forest, particularly secondary forest, as observed by single date multispectral data during peak growing season (Li & Fox, 2011). In addition, spectral characteristics of rubber trees vary in different regions or seasons, therefore, traditional spectral-based classifiers are challenging to repeat, scale, or transfer to other geographical regions. Moreover, frequent cloud coverage in the tropics presents a challenge for optical data to distinguish general forest, let alone rubber trees.

The second group of studies relies on the temporal signals of optical images to delineate rubber trees. For example, Normalized Difference Vegetation Index (NDVI) time series data from MODIS and China's Feng-Yun-3A (FY-3A) have been used to represent the phenological signatures of rubber plantations. Recently Chen et al. (2010) and Tan et al. (2010) utilized the intra-annual temporal profile of rubber plantations to delineate them in Hainan, China. This approach relied on phenological features of rubber plantations; however, the spatial resolution of MODIS is relatively coarse (250–500 m), which limits its suitability for rubber plantation mapping in fragmented landscapes. The frequent cloud cover in tropical regions also makes it difficult to construct consistent year-long MODIS time series with reliable data quality.

Therefore, the difficulty of mapping rubber plantations from optical images is two-fold: the first difficulty is the effect of frequent cloud cover on tree delineation; and the second is the similarity of spectral characteristics between rubber trees and other forest types. In comparison to optical sensors, synthetic aperture radar (SAR) can penetrate clouds and has advantages in mapping tropical forests, particularly longer wavelengths (e.g. L-band SAR) that are capable of penetrating tree canopies (Baghdadi et al., 2009). The Phased Array type L-band Synthetic Aperture Radar (PALSAR) onboard the Advanced Land Observing Satellite-1 (ALOS-1) was launched by the Japan Aerospace Exploration Agency (JAXA) in January 2006 is one such instrument. Several applications have utilized PALSAR observations to map tropical forest areas (Almeida et al., 2009; Longepe et al., 2011; Miettinen & Liew, 2011; Santoro et al., 2010; Walker et al., 2010; Xiao et al., 2010). In a previous study we combined a forest map derived from PALSAR 50-m orthorectified mosaics with a phenology-based map of rubber plantations from 250-m multi-temporal MODIS NDVI to generate a 250-m fractional cover map of rubber plantations in Hainan, China (Dong et al., 2012b). Our previous effort found that the use of cloud-free PALSAR data supported robust forest mapping and the integration of PALSAR 50-m forest maps and 250-m MODIS NDVI phenology helped to accurately map fractional cover of rubber plantation extent (Dong et al., 2012b). However, due to the heterogeneous landscapes in Hainan, the phenology information extracted from the MODIS time series included mixed pixels with signals from other land cover types, as small holder land management represents a large portion in the region. To overcome the challenge of mixed pixels, the use of time series Landsat imagery (30-m spatial resolution) could be valuable. The relatively fine resolution and free availability of Landsat images are potential sources of more phenology information at a higher spatial resolution that can substantially improve product accuracy. The advantages of multiple temporal Landsat data for land cover classification, for example, in discriminating temperate deciduous forests (Homer, Huang, Yang, Wylie, & Coan, 2004), have been well established. A simple and accurate algorithm to map rubber plantations with freely available Landsat imagery is of extreme value and urgently needed in complex landscapes across Southern China and Southeast Asia where rubber plantations continue to expand.

In this study we addressed two questions regarding mapping rubber plantations. First, is Landsat-based phenology analysis robust and capable of distinguishing rubber plantations from natural evergreen forests? Second, can delineation of rubber plantations be improved by combining PALSAR-derived forest maps with Landsat-based phenology? Our objective was to develop and apply a simple, phenology-based approach for mapping rubber plantations at a finer spatial resolution at regional scale that enables a rapid and repeated execution. The Danzhou region of Hainan Island, China was selected as the study area as this region has the largest rubber plantation area in Hainan. To achieve this objective we integrated cloud-free PALSAR and optical Landsat imagery to overcome the technical challenges faced in previous studies. This study is expected to provide a practical approach for the continental rubber plantation mapping in Southern China and Southeast Asia in the near future.

2. Materials and methods

2.1. Study area

The Danzhou region has the highest rubber production in the Hainan Province, China. According to data from the Hainan Statistical Yearbook, Danzhou produced 7.4×10^4 tons of rubber in 2011, which accounted for ~20% of rubber production in Hainan Province. It has a tropical monsoon climate with an annual mean temperature of approximately 25 °C and annual accumulated precipitation between 1800 and 2000 mm. The region is located in western Hainan and the influences of typhoons are relatively small compared with eastern regions of Hainan. Elevation increases from <50 m in the northwest to 752 m in the southwest (Fig. 1). Natural forests in Danzhou are mainly evergreen, while rubber trees show deciduous characteristics. Defoliation is an adaptation of rubber trees to low temperature and/or dry monsoon. When rubber trees were introduced in British Malaysia in the 20th century, the trees were considered unsuitable for northern parts of the tropics such as Hainan Island. However, rubber germplasm improvement enhanced the capability to adapt to frequent typhoons and low winter temperature (Li & Fox, 2012).

2.2. PALSAR data and pre-processing

PALSAR 50-m Orthorectified Mosaic data were used to generate a forest map. The PALSAR mosaic data are freely available through the ALOS Kyoto and Carbon Initiative (ftp://ftp.eorc.jaxa.jp/pub/ALOS/ftp/KC50/). The data have been geometrically rectified using a 90-m digital elevation model (DEM) and geo-referenced to geographical latitude and longitude coordinates (Longepe et al., 2011). Detailed algorithms and data processing including calibration and validation were reported in Shimada et al. (2008), Shimada and Ohtaki (2010).

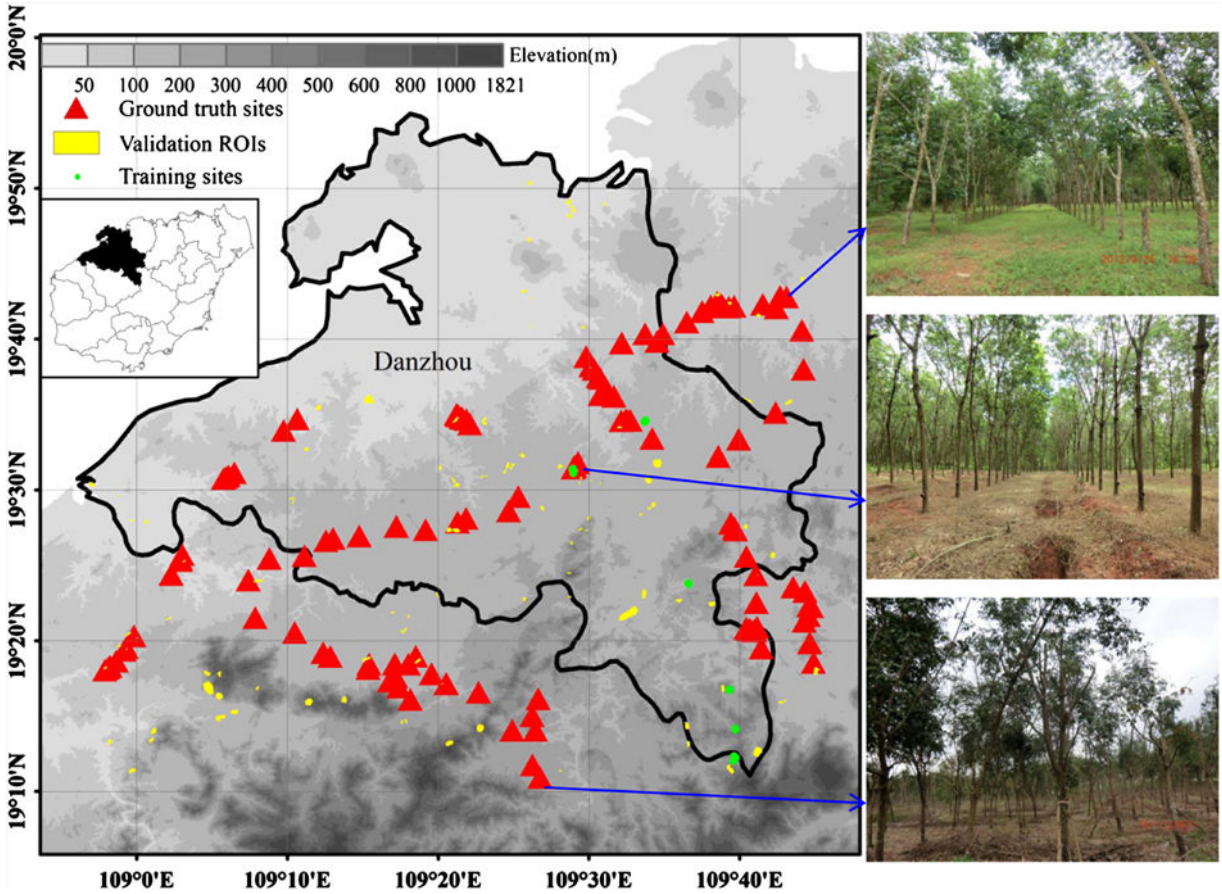

Fig. 1. The location of Danzhou City in the Hainan Province of China and its topography. Danzhou is a major agroforestry region with the highest density of rubber plantation on Hainan Island. The red triangles show the locations of reference photos from our field trips in 2011 and 2012. The yellow polygons show the distribution of the ROIs for the validation of PALSAR-based land cover map and the resulting rubber plantation map. The photos on the right side show rubber plantations in northern, central and southern parts of the study area. (For interpretation of the references to color in this figure legend, the reader is referred to the web version of the article.)

We obtained 50-m mosaics with Fine Beam Dual polarization (FBD) observational mode between July-Oct. 2009, which has two polarizations (HH and HV). The HH and HV polarization data were converted from amplitude into the normalized radar cross-section backscatter (dB) according to the following equation (Rosenqvist, Shimada, Ito, & Watanabe, 2007):

$$\sigma^0(dB) = 10 \times \log_{10} DN^2 + CF \quad (1)$$

where σ^0 is the backscattering coefficient, *DN* is the digital number value of pixels in HH or HV; and *CF* is the absolute calibration factor of -83. Besides HH and HV polarization images, two composited images (the ratio and difference of HH and HV) were also generated, since these indices have been shown to be valuable for land cover classification (Dong et al., 2012a; Miettinen & Liew, 2011; Wu, Wang, Zhang, Zhang, & Tang, 2011).

2.3. Landsat data and pre-processing

In order to capture the phenological characteristics of rubber trees and other land cover types, 18 standard level-one terrain-corrected (L1T) products of Landsat TM and ETM+ images (path/row 124/47) circa 2009 (from 2007 to 2012) were obtained from the USGS Earth Resources Observation and Science (EROS) Data Center (Table 1). Radiometric and geometric corrections have been conducted, and the overall geometric fidelity has also been fitted using ground control points and a digital elevation model in Level 1 T Landsat products (NASA Goddard Space Flight Center, 2011). We conducted atmospheric correction and acquired surface reflectance by using the Landsat Ecosystem Disturbance Adaptive Processing System (LEDAPS) routine, which uses the MODIS 6S radiative transfer approach to retrieve surface reflectance (Masek et al., 2006; Vermote et al., 1997). Three vegetation

Table 1
A list of Landsat TM/ETM+ images used in this study. All the images are with the same orbit number (Path/Row 124/47), and have relative limited cloud cover in the study area. Cloud coverage values and SLC-off strips are not processed as we used the samples (12 rubber plantation samples and 13 natural forest samples) outside the striping for phenology analysis.

Acquired date	DOY	Sensor	Acquired year
January 6	6	Landsat 7 ETM+	2008
February 25	56	Landsat 7 ETM+	2009
February 28	59	Landsat 7 ETM+	2010
March 5	65	Landsat 7 ETM+	2012
March 10	70	Landsat 7 ETM+	2008
March 16	75	Landsat 5 TM	2007
March 24	83	Landsat 5 TM	2010
April 1	91	Landsat 7 ETM+	2010
May 8	129	Landsat 7 ETM+	2012
June 1	152	Landsat 7 ETM+	2009
July 6	187	Landsat 7 ETM+	2010
August 20	232	Landsat 7 ETM+	2009
September 21	262	Landsat 7 ETM+	2009
October 31	304	Landsat 5 TM	2009
December 10	344	Landsat 7 ETM+	2009
December 13	347	Landsat 7 ETM+	2010
December 26	360	Landsat 7 ETM+	2009
December 29	363	Landsat 7 ETM+	2010

indices were calculated using the surface reflectance, including NDVI (Tucker, 1979), Enhanced Vegetation Index (EVI) (Huete, Liu, Batchily, & vanLeeuwen, 1997; Huete et al., 2002), and Land Surface Water Index (LSWI) (Xiao, Zhang, Hollinger, Aber, & Moore, 2005; Xiao et al., 2004) with the following equations,

$$NDVI = \frac{\rho_{NIR} - \rho_{red}}{\rho_{NIR} + \rho_{red}} \quad (2)$$

$$EVI = 2.5 \times \frac{\rho_{NIR} - \rho_{red}}{\rho_{NIR} + 6 \times \rho_{red} - 7.5 \times \rho_{blue} + 1} \quad (3)$$

$$LSWI = \frac{\rho_{NIR} - \rho_{MIR}}{\rho_{NIR} + \rho_{MIR}} \quad (4)$$

where ρ_{blue}, ρ_{red}, ρ_{NIR}, and ρ_{MIR} are the surface reflectance values of the Band 1 (Blue, 0.45–0.52 mm), Band 3 (Red, 0.63–0.69 mm), Band 4 (near-infrared, NIR for short hereafter, 0.76–0.90 mm) and Band 5 (Shortwave-infrared, 1.55–1.75 mm) in Landsat TM/ETM+ sensors, respectively.

2.4. Ground reference data for algorithm training and product validation

2.4.1. Geo-referenced field photos (points of interest)

We conducted field surveys of rubber plantations and other land cover types in 2011 and 2012. Using a Casio Exolim EX-H20G GPS camera, 482 geo-referenced field photos in the study area were collected for training and validation of the classification routine. All field photos capture specific information about land cover types and the sampling strategy focused on rubber plantations. The locations of these ground truth samples are shown in Fig. 1. All the field photos are stored and managed in the Global Geo-Referenced Field Photo Library (http://www.eomf.ou.edu/photos/), which is a data portal that is open to the public and the science community. Users can upload, manage, and download field photos in the platform. As of October 2012, there were 1,200 photos available for Hainan Island (Fig. 1). We processed all the field photos in the study area as kml files, which we hereinafter refer to as points of interest (POIs); all these POIs were geo-linked with Google Earth to help digitize regions of interest (ROIs) for algorithm training and product validation (Fig. 2). Although this study used Landsat and PALSAR imagery from circa 2009 for mapping rubber plantations, the ground truth data from 2011 to 2012 are suitable as rubber trees grow for many years with consistent seasonal phenology.

2.4.2. Regions of interest (ROIs) for algorithm training and product validation

Although we collected abundant geo-referenced field photos, the pixel samples where the photos are located are not sufficient for both algorithm training and rigorous map validation. We used high spatial resolution imagery within Google Earth to extrapolate the POIs into ROIs. The field photos provide reference information for the interpretation and digitalization of ROIs in Google Earth. This approach was used in our previous studies and proved to be effective (Dong et al., 2012a, 2012b). Some previous studies have also used Google Earth for validation of land classification considering its geometric accuracy and the fine spatial resolution of imagery (Benedek & Sziranyi, 2009; Cohen, Yang, & Kennedy, 2010; Huang et al., 2010; Montesano et al., 2009; Potere, 2008).

By cross-validating the Google Earth images and the geo-referenced field photos in the study area, a group of ROIs was developed as training samples for the phenology feature analysis of rubber plantations and natural evergreen forests. This included 14 rubber ROIs (884 pixels), and 15 natural evergreen forest ROIs (2,441 pixels). The separability scores of the ROIs were calculated by using the

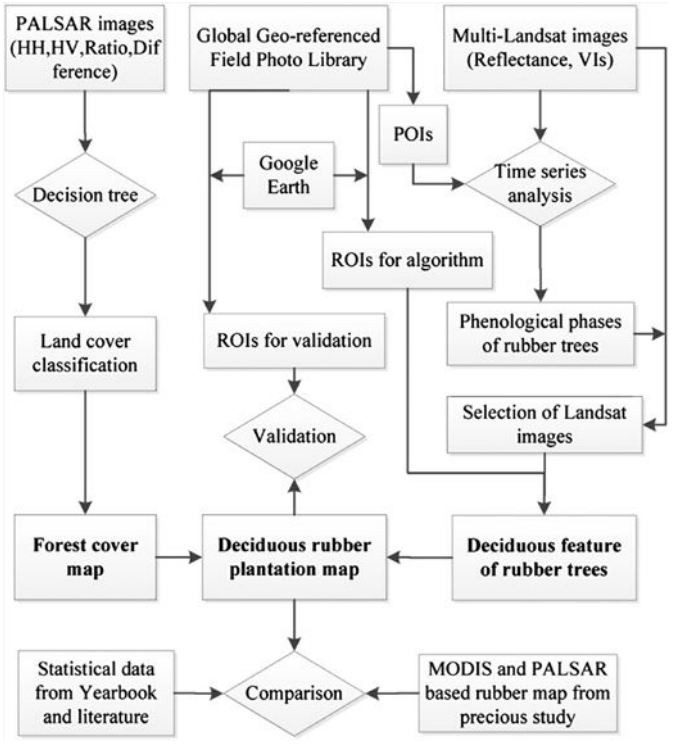

Fig. 2. The workflow for mapping rubber plantation based on 50-m PALSAR orthorectified mosaic product and 30-m Landsat images. PALSAR-based forest/tree mapping and Landsat-based phenology feature extraction of rubber trees are conducted independently. Three groups of ground truth data are used: (a) the points of interest (POIs) are used for the phenology phase extraction (13 natural forest ones and 12 rubber plantation ones) by using multi-temporal Landsat images, (b) the training regions of interest (ROIs) are used to acquire the phenology feature of rubber plantation based on the Landsat images in the foliation stage, and (c) the validation ROIs are used for accuracy assessments of land cover classification and the rubber plantation map.

Jeffries-Matusita (J-M) distance (Eq. (5)) (Richards & Jia, 1999) between the two ROIs with all bands as inputs.

$$JM_{ij} = \sqrt{2(1 - e^{-a})} \quad (5)$$

where JM_{ij} is the J-M distance between signatures i and j, and a is the Bhattacharyya distance, which is calculated using the following equation:

$$a = \frac{1}{8}\left(U_i - U_j\right)^T \left[\frac{C_i + C_j}{2}\right]^{-1} \left(U_i - U_j\right) + \frac{1}{2} Ln \left[\frac{\left|1/2\left|C_i + C_j\right|\right|}{\sqrt{|C_i||X||C_j|}}\right] \quad (6)$$

where i and j represent the two classes of interest, T is transpose, C_i is the variance-covariance matrix of signature i, U_i is the mean vector of signature i, and $|C_i|$ is the determinant of C_i. The J-M distance value of the ROI pairs was larger than 1.9. As a commonly used rule, a J-M distance value above 1.9 means the separability between the two classes is good (Richards & Jia, 1999). Therefore, the rubber plantation and natural forest ROIs in this study have good separability and are reasonable for use as training samples.

Another group of ROIs for product validation with five main land cover types were generated, namely: rubber plantation, natural forest, cropland, water, and built-up land. As the Google Earth imagery in the area spanned from 2000 to 2012 and some images were out of date in the study area, we only created the ROIs with imagery from circa 2009 to match the acquisition period of Landsat imagery. Image dates, phenology, and ROI size were also considered during

the process of ROI creation. A total of 113 polygon ROIs (~29,000 pixels) were created to conduct thorough accuracy assessments for not only PALSAR-based land cover classification, but also the further PALSAR/Landsat-based rubber plantation map using confusion matrix, including 33 rubber ROIs (5470 pixels), 29 natural evergreen forest ROIs (10,229 pixels), 29 cropland ROIs (4288 pixels), 6 water ROIs (4789 pixels), and 16 ROIs (4586 pixels) for other land cover. The ROIs are widely distributed in the study area (Fig. 1).

2.5. PALSAR-based forest cover mapping

In our previous study, we used PALSAR 50-m mosaics to generate a map of forest and non-forest in Southeast Asia (Dong et al., 2012a). As Hainan Island belongs to the Southeast Asia region and has the same tropical landscapes, we used the same approach to generate the forest/non-forest map in 2009 in Hainan Island, China. The four land cover types, including water, forest, cropland, and others, have different PALSAR backscatter signatures. For example, forests have higher backscatter values than water and cropland. According to the backscatter differences of the four land cover types, a land cover map in Danzhou was generated (Fig. 3) with the same approach reported in our previous publication (Dong et al., 2012a).

This PALSAR-based 50-m forest map was used as a mask to overlay with the phenology information of rubber trees in an effort to produce a rubber plantation map. The 50-m forest mask was extracted from the land cover classification result (Fig. 3); and resampled to 30-m to match the Landsat spatial resolution. Both rubber plantations and natural evergreen forests belong to the general forest class as mapped by the PALSAR-based approach (Dong et al., 2012a).

2.6. Landsat-based phenology analysis

Rubber trees in Hainan are sensitive to cold temperatures and defoliate in winter, which is a unique characteristic that is different from natural forests and other cash forests such as lichee and longan (Chen et al., 2010). That is the reason that the rubber plantations in Hainan Island have deciduous characteristics while the rubber plantations in equatorial regions don't.

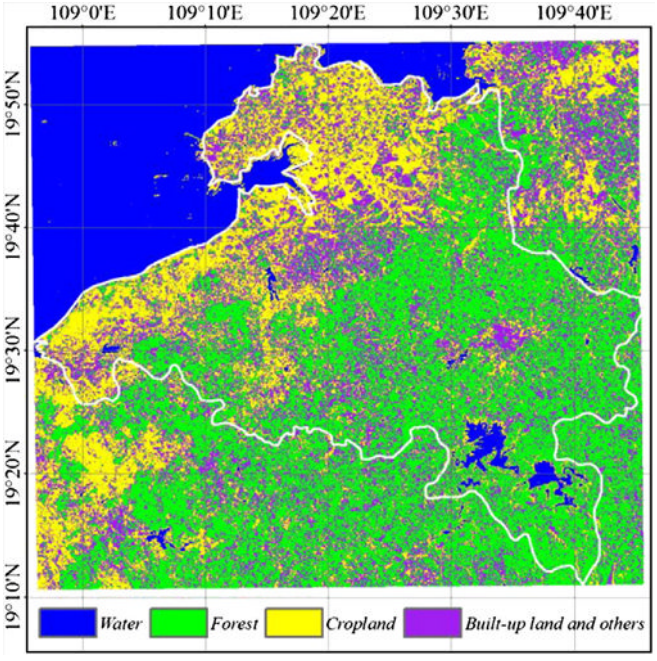

Fig. 3. The 50-m land cover map in 2009, derived from PALSAR 50-m orthorectified mosaic images. It has four land cover types (forest, cropland, water, built-up land) and unclassified category.

Temporal profiles of three vegetation indices (NDVI, EVI and LSWI) from 18 Landsat images were constructed to examine the phenology of rubber plantations and natural evergreen forests (Fig. 4). Twelve representative sites were selected for rubber plantations and another thirteen sites for natural evergreen forests. Multiple years of images from 2007 to 2012 (15 images from 2008 to 2010) were collected to represent the seasonal variations of the three vegetation indices and NIR reflectance as it is difficult to acquire temporal Landsat TM images in this region due to frequent cloud cover and data availability. Scan Line Corrector (SLC) issues were circumvented by extracting pixels outside of striping lines.

Based on the intra-annual temporal analysis of vegetation indices, we found that rubber and natural evergreen forests are distinguishable by Landsat imagery in two periods: (1) late February to March (defoliation period) and (2) late March to April (foliation period). The detailed phenology description is given in Section 3.1.

2.7. Rubber plantation delineation by integrating PALSAR and Landsat

For regional mapping, Landsat TM images in either defoliation or foliation stages can support rubber plantation identification. As there were no good-quality images available in the defoliation stage, we used images in the foliation phase for rubber plantation delineation. Two Landsat 5 TM L1T images (Path/Row 124/46 and 124/47) in March 24, 2010 (in the foliation stage of rubber trees, Fig. 4) were used for the case study in Danzhou. This imagery in the foliation phase clearly shows the rubber plantations (Fig. 5a), which appear light green in the false color composite map (R/G/B = Band 5/4/3). We found that images from unique phenological phases have better performance than those from other periods, for example, rubber plantations and natural evergreen forests have similar optical characteristics in an image acquired in June (Fig. 5b). The three vegetation indices (NDVI, EVI, and LSWI) and the six spectral bands were stacked for phenology feature extraction of rubber plantations.

The rubber plantation map was generated by combining the PALSAR-based forest layer and the phenology feature of rubber trees (Fig. 2). The 30-m forest map derived from PALSAR images has been described in Section 2.5. The phenological feature map of rubber plantations at 30-m resolution was extracted based on the results of statistical analysis of band reflectance and vegetation indices in the defoliation stage (see Section 3.1). These two maps were combined by using the intersection tool in ArcGIS software.

2.8. Validation and comparison

The resultant map of rubber plantations at 30-m spatial resolution was evaluated by using a confusion matrix based on the ROIs for validation. In addition, the 30-m rubber plantation map in this study was compared with the rubber fractional map from our previous study in Hainan Island by integrating PALSAR and MODIS (Dong et al., 2012b). The rubber plantation areas and the spatial distributions in the entire Danzhou were compared; also, Pearson's correlation was conducted between two rubber plantation fractional maps from a random sample of pixels ($n = 3556$). For the comparison, the PALSAR and Landsat-based binary rubber plantation map was aggregated into fractional map to match the PALSAR and MODIS-based rubber plantation fractional map.

3. Results

3.1. Forest map derived from PALSAR 50-m orthorectified mosaic imagery

The resulting PALSAR-based land cover map has a high accuracy based on the ROIs for validation. The overall accuracy was 87% and kappa coefficient was 0.80. The both user's accuracy and producer's

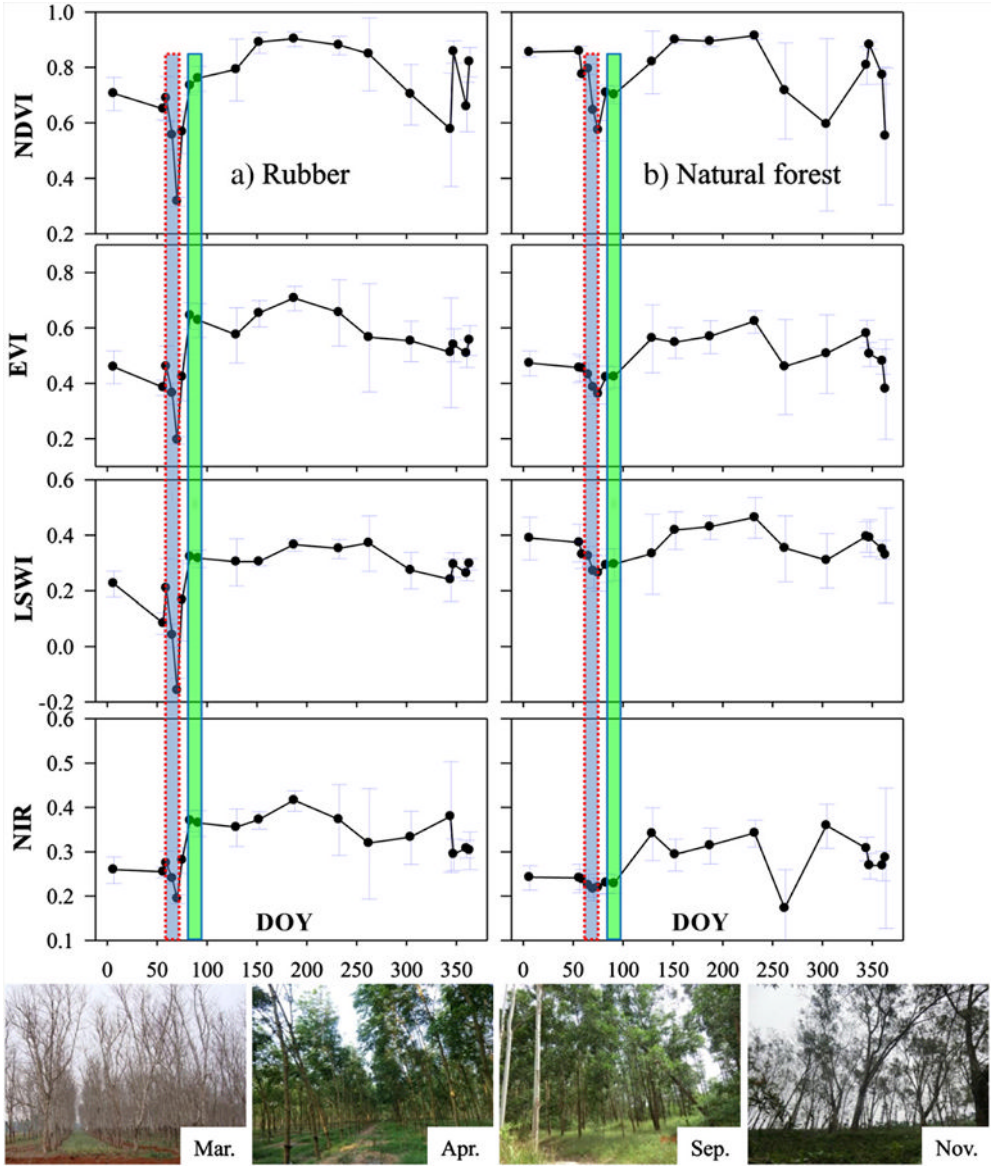

Fig. 4. The temporal profiles of time series Landsat NDVI, EVI, LSWI and near-infrared (NIR) reflectance for (*a*) rubber plantations, and (*b*) natural forests. Twelve points of interest (POIs) were extracted for rubber plantations and 13 POIs for natural forests. The points and error bars show their average and standard deviation (SD) values. Rubber plantations and natural forests are evidently different in two typical phenology phases: defoliation (the brown long and narrow boxes) and foliation (the green long and narrow boxes). The four field photos in different periods (March 16, 2008, April 24, 2012, September 10, 2012, and November 16, 2011 from left to right) show the intra-annual changes of rubber trees' canopy. The photos were not taken in the same regions but they were all close to the selected points. It is clear that the leaves of rubber trees fall off greatly in late February and early March, and the canopy recovers rapidly in April. The high SD values from June to October show data quality is poor in the period due to frequent cloud covers.

accuracy of the forest category were higher than 93% (Table 2). Therefore, the forest map can serve as a reliable base map for rubber plantation delineation. The categories of cropland and other land cover had lower accuracies than those of forest and water; for example, the other land cover category had a low user's accuracy (71%) and producer's accuracy (64%) due to the complex backscatter of built-up areas. However, this is not of concern as the focus is forest in this study.

3.2. Phenological phases of deciduous rubber trees as observed from Landsat

Fig. 4 shows the seasonal dynamics of three vegetation indices and NIR reflectance from rubber plantations and natural evergreen forests. In the peak period of the plant growing season (e.g., mid-summer), rubber plantations had similar level of vegetation indices to that of natural evergreen forests. In the late winter season, rubber trees defoliated substantially in late February or early March (see the photos in Fig. 4). The canopy density decreased to a low level by as much as 20% or less which was reported in an earlier study (Chen et al., 2010). Rubber trees underwent rapid foliation and canopy recovery from late March to April. Rubber plantations had higher NIR and EVI values than natural evergreen forests in the foliation stage (Fig. 4), which suggests that rubber plantations can be separated from natural evergreen forests.

The spectral signature analyses based on the training ROIs and the image acquired during the foliation stage (Fig. 5a) showed that rubber trees and natural evergreen forests have different phenological characteristics during this period (Fig. 6). NIR reflectance values were higher in rubber plantations (0.347 ± 0.027) than in natural evergreen forests (0.245 ± 0.019). Similarly, EVI values were also higher in rubber plantations (0.595 ± 0.056) than in natural evergreen forests (0.437 ± 0.038). The other VIs examined (NDVI, LSWI) had less ability to separate rubber plantations from natural evergreen forests. NIR performed a larger separability than EVI (Fig. 6). Therefore, we used a

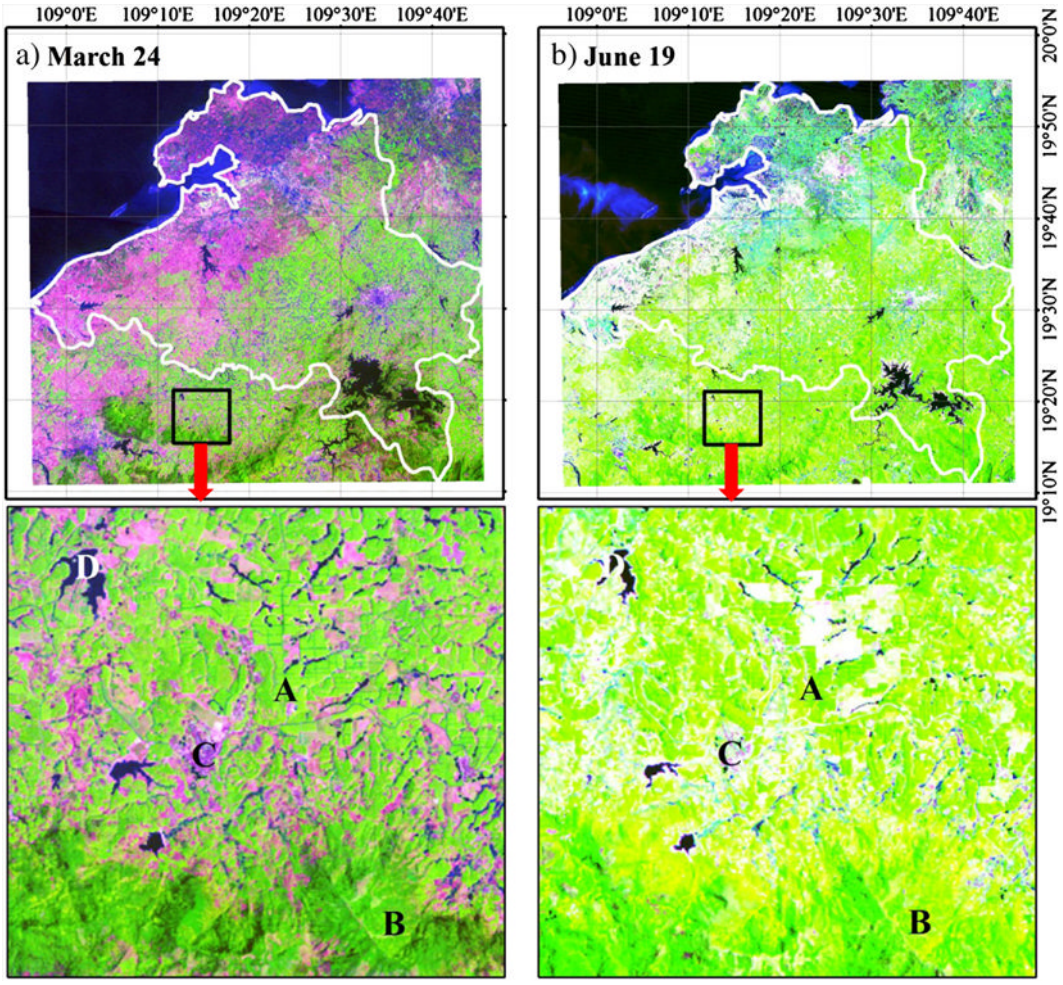

Fig. 5. The false color composition map (R/G/B = Band 5/4/3) of Landsat TM5 images (*a*) — March 23, 2010, and (*b*) — June 19, 1995. The below zoom-in images of a small area show that rubber plantation is readily visible as light green patches in the foliation stage image (*a*), but rubber plantation and natural forest are indistinguishable in (*b*) which is in neither defoliation nor foliation stage. Several classes of interest were marked in the zoom-in images, including rubber ('A'), natural forest ('B'), built-up land ('C'), and water ('D').

NIR reflectance > 0.29, the mean value of the lower rubber NIR reflectance value (0.347 - 0.027) and the higher forest NIR reflectance value (0.245 + 0.019), as the threshold value for phenological feature extraction of rubber plantations.

3.3. The rubber plantation map and accuracy assessment

By combining the PALSAR-based forest mask (Fig. 7a) and Landsat-based rubber phenology (Fig. 7b), a rubber plantation map was generated (Fig. 7c). The rubber plantation area in Danzhou City was estimated at 594 km^2 in 2009, which was slightly higher than the estimate (590 km^2) in 2007 from a previous study (Cao, 2008). There was no precise reference data available in 2009 for comparison; however, the rubber plantation area was estimated to be more than 600 km^2 as the private rubber plantations continued to grow rapidly in recent years (Xu, 2010). In this study, omission of young rubber trees might exist, as young rubber trees have overlapping spectral characteristics with the background landscape (Li & Fox, 2012).

The resulting rubber plantation map has a high accuracy according to the confusion matrix by using the ground truth ROIs. The overall accuracy is 92% and the kappa coefficient is 0.88 (Table 3). The interpretation accuracy of rubber plantations is high with both user's and producer's accuracies at 96%.

Table 2
Accuracy assessment of the land cover classification map based on PALSAR 50-m mosaic data in this study. The validation samples of the "forest" category include both natural forest and rubber plantation, and the samples of the "others" category are mainly built-up land.

	Class	Ground truth samples (pixels)				Total classified pixels	Prod. acc.
		Forest	Cropland	Water	Others		
Classified results	Forest	14,960	252	0	938	16,150	93%
	Cropland	61	2868	199	351	3479	82%
	Water	0	39	4584	19	4642	99%
	Others	678	1129	6	3278	5091	64%
Total ground truth pixels		15,699	4288	4789	4586	29,362	
User acc.		95%	67%	96%	71%		

Overall accuracy is 87%; kappa coefficient is 0.80.

3.4. Comparison with the rubber plantation map derived from PALSAR and MODIS imagery

The PALSAR/Landsat-based rubber plantation map and the PALSAR/MODIS-based rubber plantation map have high consistency in spatial distribution, as shown in Fig. 8a and b; however the PALSAR/Landsat-based map from this study has more detail in spatial distribution. For example, a zoom-in analysis (Fig. 8d-f) shows that the PALSAR/Landsat-based rubber plantation map provides higher spatial configuration and spatial detail compared to that of the PALSAR/MODIS map, especially in the regions where the PALSAR/MODIS map has a low rubber density.

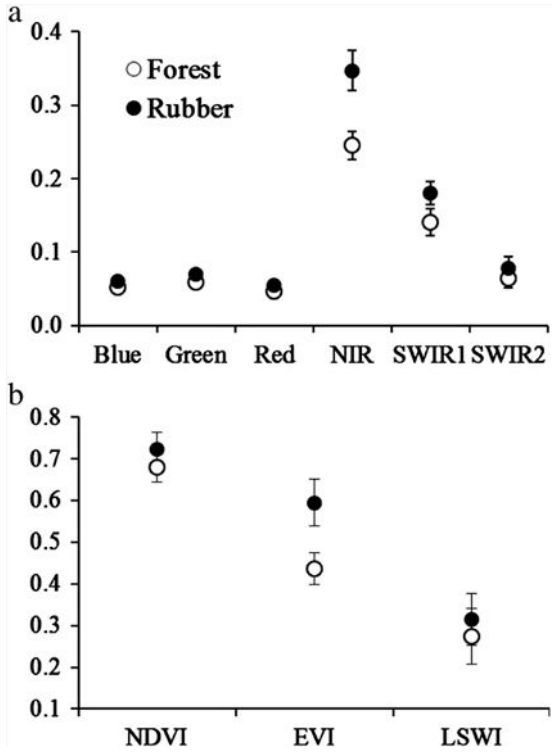

Fig. 6. Signature analysis of (*a*) the reflectance of spectral bands and (*b*) the vegetation indices (NDVI, EVI and LSWI) for rubber plantations and natural forests based on the Landsat 5 images in March, 2010. Rubber plantation and natural forests have distinctive values in NIR and EVI.

The correlation coefficient between these two maps from a sample of pixels is 0.88 ($p < 0.001$, $n = 3556$). The PALSAR/MODIS-based rubber plantation map has an area estimate of 711 km^2, which is approximately 20% larger than that of PALSAR/Landsat-based map from this study (594 km^2). The regression analysis between these two maps also shows the discrepancy between these maps (Fig. 8c). The difference is likely to be caused by sub-pixel level spectral mixture issues in the MODIS-based analysis. The study area in this paper has complex landscapes and most land parcels are in small size. A MODIS pixel (250-m resolution) is more likely to contain several land cover types than does a TM pixel (30-m resolution), and the phenology information from MODIS imagery is thus complicated by the issue of mixed pixels. The use of phenology information from Landsat imagery clearly resulted in higher accuracy in mapping rubber plantations.

4. Discussion

4.1. Primary findings and potential for regional rubber mapping

The results from this study showed that the finer spatial resolution Landsat imagery provides more spatial details about the extent and spatial configuration of rubber plantations than MODIS imagery (Dong et al., 2012b; Li & Fox, 2012). The distinct difference in phenology between rubber plantations and natural evergreen forests in the study area occurs in two specific phenological phases (Fig. 5). These two phenological phases are unique and can be used to delineate rubber plantations from natural evergreen forests simply by selecting and using strategic images in one of these two phenological phases. In defoliation phase (February to Early March) rubber plantations have a canopy with little or no green leaves and low NDVI/EVI/LSWI values due to defoliation, while evergreen forests have only slight change in canopy coverage with high VI values. In foliation phase (Late March to April) rubber trees have rapid foliation (new leaf emergence) and

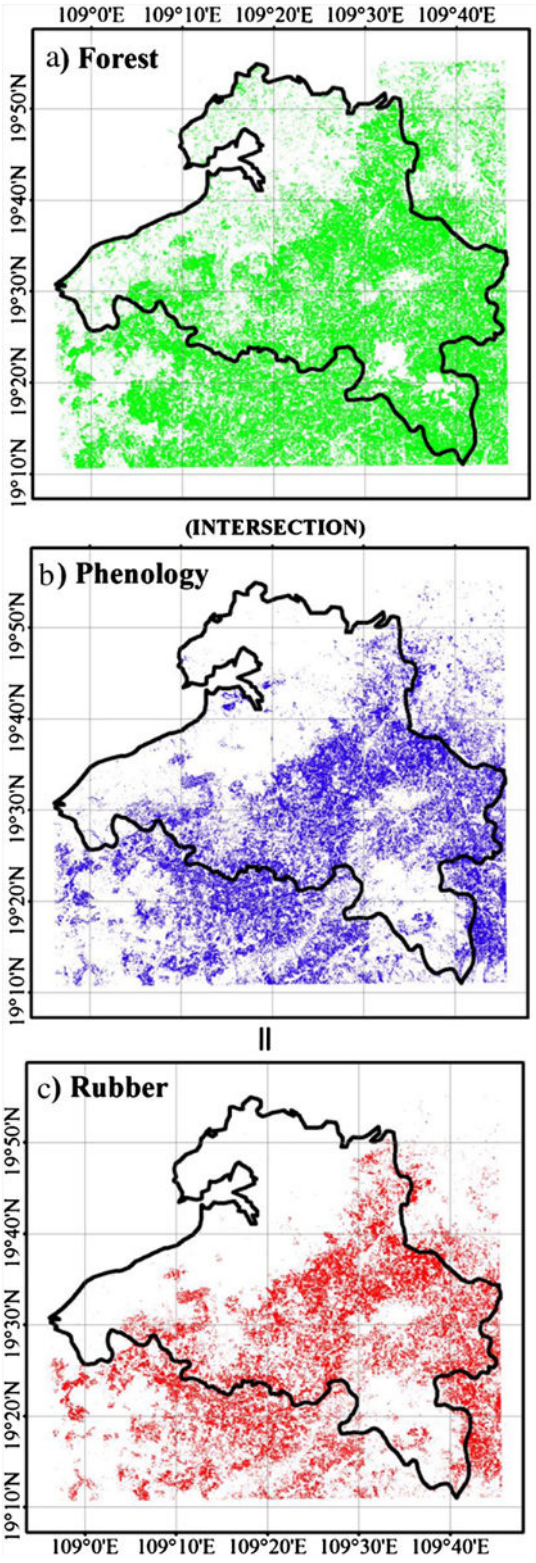

Fig. 7. (*a*) The forest layer with a 30-m resolution, which was derived from the 50-m PALSAR-based land cover map (Fig. 3) and then resampled into Landsat scale; (*b*) the spatial distribution of the unique phenology feature (near-infrared reflectance > 0.29) of rubber plantations in foliation stage by using the selected image in certain phenology phase (March 24, 2010). (*c*) The resultant rubber plantation map with 30-m resolution by combining the forest layer (*a*) and the rubber phenology feature (*b*).

canopy recovery. During this phase new leaves have higher spongy mesophyll content, which results in high reflectance in near infrared bands. In comparison, natural evergreen forest has relatively lower

Table 3
Accuracy assessment of the rubber plantation map by integrating PALSAR-based forest base map and Landsat-based phenology feature in this study. The validation samples of the "others" category are the sum of the "cropland", "water" and "others" categories used in Table 2.

	Class	Ground truth samples (pixels)			Total classified pixels	Prod. acc.
		Rubber	Natural forest	Others		
Classified results	Rubber	5225	220	13	5458	96%
	Natural forest	135	9386	1110	10,631	88%
	Others	110	623	12,540	13,273	94%
Total ground truth pixels		5470	10,229	13,663	29,362	
User Acc.		96%	92%	92%		

Overall accuracy is 92%; kappa coefficient is 0.88.

NIR values because the canopy is composed of leaves of different ages and more mature leaves have lower NIR values.

This work showed that deciduous rubber plantations can be identified and mapped rapidly and effectively with images acquired in designated phenological phases (defoliation or foliation). That led to a higher resolution rubber plantation map by using PALSAR and Landsat in a certain phenological phase (e.g., the end of March in this study). Once the defoliation or foliation periods of rubber are defined for a given region and temporal window, single date imagery can support the rubber plantation mapping at regional scale. That can transform the 'temporal' analysis into the 'static' analysis, and greatly simplify rubber plantation mapping. This study emphasizes the utility of phenology-based image selection for land cover classification, especially for dynamic or deciduous vegetation. We also found that the presence of cloud cover is frequent from June to October and there are few good-quality images available in Hainan (Fig. 2). The approach detailed here can overcome this obstacle as the defoliation and foliation stages are not concordant with the cloudy period.

Landsat-based phenological analysis provides finer spatial information than MODIS, because MODIS pixels (250-m or 500-m) often contain mixed types of land covers. In our previous MODIS-based study, temporal profiles of NDVI, LSWI, and EVI showed an evident decrease in the defoliation stage (late February and early March); particularly, the LSWI value of evergreen forest is always higher than 0 for the whole year while that of deciduous rubber plantation is lower than 0 in some periods of a year (Xiao, Biradar, Czarnecki, Alabi, & Keller, 2009). However, MODIS data cannot detect the rapid recovery of rubber trees in the foliation stage due to mixed land cover types within 250-m or 500-m pixels (Dong et al., 2012b), while Landsat can capture a more specific intra-annual phenology at 30-m spatial resolution (Fig. 4).

In this study, we used PALSAR data to extract a tree/forest base map by using a physical approach. Landsat images were not used in the process of forest mapping. The reason is that the PALSAR based forest map is more operational for a large area application, while Landsat and spectral-based approaches are limited when used for other regions or seasons (times). In addition, a single PALSAR L-band backscatter image has proven useful in mapping rubber, oil palm, coconut and wattles plantations (Miettinen & Liew, 2011), and the input of this information would improve the capability to delineate rubber plantation in future studies.

4.2. Uncertainty analysis

Rubber trees in the study area (northern tropical zone) have distinct defoliation and foliation phases, which are common characteristics of deciduous forests. The phenology of rubber trees in different latitudes could have some temporal inconsistencies with the findings described here. Also, inter-annual shifts in phenological phases caused by climate variability might alter the required data acquisitions for delineating rubber plantations. Other factors such as slope, aspect, or rubber variety also might be different in other regions. Therefore, the thresholds used in this study might need

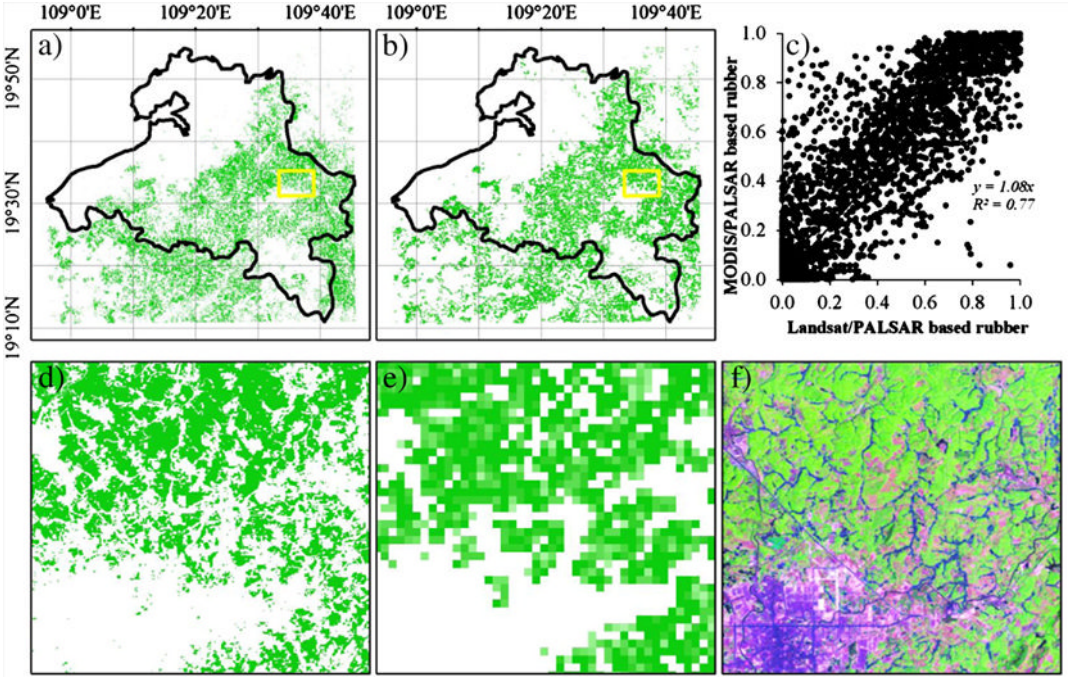

Fig. 8. Comparison between (*a*) the rubber plantation map by using the PALSAR/Landsat-based approach and (*b*) the rubber plantation map by using the PALSAR/MODIS-based approach (Dong et al., 2012b). (*c*) The scatterplot of two rubber plantation fractional maps from a random sample of pixels. The PALSAR/Landsat-based area percentage map is acquired by aggregating the binary rubber map (*a*) to an area percentage map at MODIS-scale. The rubber area estimates from both results are significantly correlated. The equation of the linear fitting line in (*c*) is $y = 1.08x$ ($R^2 = 0.77$, $p < 0.001$, $n = 3556$). (*d*) The zoom-in image extracted from (*a*), and (*e*) the zoom-in image extracted from (*b*), showed PALSAR/Landsat-based rubber map has a higher accuracy and resolution than that form MODIS/PALSAR, by referring to (*f*) the false color composite map of Landsat TM image (extracted from Fig. 5*a*).

adjustments in other regions. As Southeast Asia has the largest proportion of rubber plantations in the world (FAO, 2010), a systematic investigation about regional phenology differences of rubber trees will help to realize rubber plantation mapping at the continental scale.

In addition, this study focuses on mature rubber plantations. Young rubber plantations (≤5 years according to the experiences of local experts from the Rubber Research Institute in Danzhou City) could be missed due to differences in spectral characteristics (Benedek & Sziranyi, 2009), as the canopy of young rubber trees is small and most young rubber plantations are surrounded by other vegetation or bare land. That could be one reason that our rubber plantation area estimate is lower than the official statistic. Comparison studies of spectral characteristics of rubber plantations at different ages should be considered in the future.

4.3. Ground truth data

Effective ground truth samples are a critical concern in land cover and land use change studies. However, the reliability of ground reference data is often ignored to some extent in the accuracy assessment of land cover mapping and change detection, which can be a source of considerable error and misinterpretation (Foody, 2010). Field campaigns and high resolution imagery are common approaches to acquire ground truth data. Usually, an extensive field survey is unrealistic due to cost and logistical constraints. Very high resolution imagery (<1 m) is expensive and users tend to use less than ideal data for reference purposes (Foody, 2010). Note that every year thousands of researchers in the scientific communities (ecologists, geographers, biological surveyors, and so on) carry out field visits for different purposes or projects, and many repeated field surveys have been conducted without data sharing. One reason for the information sharing gap is the lack of an effective data portal to organize and manage spatial datasets. In this study, we showcased an application of the Global Geo-Referenced Field Photo Library (Xiao, Dorovskoy, Biradar, & Bridge, 2011). The abundant high quality field photos (>50,000 until December of 2012) in the Field Photo Library are expected to provide effective support for many research fields such as land cover and land use change, biogeography, and others.

5. Conclusion

Southeast Asia, especially southern China, has undergone an intensive land use conversion from natural tropical rainforests to industrial forests or plantations in recent decades. Rubber trees are one of the most important industrial forest species. However, an accurate rubber plantation map is still unavailable, which limits our understanding of environmental and ecological effects of rubber expansion and forest management. In this study, we explored the capability of a simple and phenology-based strategy in rubber plantation mapping in Hainan, China, a hotspot of rubber plantation expansion, by integrating a forest map from PALSAR data and rubber tree phenology features from Landsat imagery. We found that the unique phenological characteristics of rubber plantations can be retrieved in two critical phenological phases: the defoliation and foliation stages. Furthermore, the Landsat imagery in these key phenological phases can effectively support rubber plantation mapping at 30-m spatial resolution at a regional scale, which facilitates rubber plantation delineation and mapping in sub-tropical and northern parts of tropical regions. However, other factors, such as the spatial heterogeneity of regional phenology, should also be considered and incorporated when the approach used in this study is employed in other regions.

Acknowledgments

This study was supported by the NASA Land Use and Land Cover Change program (NNX09AC39G, NNX11AJ35G), the US National Science Foundation EPSCoR program (NSF-0919466), and the Fundamental Research Funds for Rubber Research Institute, Chinese Academy of Tropical Agricultural Sciences (1630022011012, 1630022012019). Landsat imagery is available from the U.S. Geological Survey (USGS) EROS Data Center. The original PALSAR data are provided by JAXA as the ALOS product. We thank two reviewers for their thoughtful and constructive review and comments on earlier version of the manuscript. We thank Melissa Brown for her English editing and comments.

References

Almeida, R., Shimabukuro, Y. E., Rosenqvist, A., & Sanchez, G. A. (2009). Using dual-polarized ALOS PALSAR data for detecting new fronts of deforestation in the Brazilian Amazonia. *International Journal of Remote Sensing*, *30*, 3735–3743.

Baghdadi, N., Boyer, N., Todoroff, P., El Hajj, M., & Begue, A. (2009). Potential of SAR sensors TerraSAR-X, ASAR/ENVISAT and PALSAR/ALOS for monitoring sugarcane crops on Reunion Island. *Remote Sensing of Environment*, *113*, 1724–1738.

Benedek, C., & Sziranyi, T. (2009). Change detection in optical aerial images by a multilayer conditional mixed Markov model. *IEEE Transactions on Geoscience and Remote Sensing*, *47*, 3416–3430.

Cao, J. (2008). *Compare study on nutrient ecology of clone PR107 in DanZhou, Hainan.* Haikou: Hainan University.

Chen, H., Chen, X., Chen, Z., Zhu, N., & Tao, Z. (2010). A primary study on rubber acreage estimation from MODIS-based information in Hainan. *Chinese Journal of Tropical Crops*, *31*, 1181–1185.

Cohen, W. B., Yang, Z. G., & Kennedy, R. (2010). Detecting trends in forest disturbance and recovery using yearly Landsat time series: 2. TimeSync — Tools for calibration and validation. *Remote Sensing of Environment*, *114*, 2911–2924.

Dong, J., Xiao, X., Sheldon, S., Biradar, C., Duong, N. D., & Hazarika, M. (2012a). A comparison of forest cover maps in Mainland Southeast Asia from multiple sources: PALSAR, MERIS, MODIS and FRA. *Remote Sensing of Environment*, *127*, 60–73.

Dong, J., Xiao, X., Sheldon, S., Biradar, C., & Xie, G. (2012b). Mapping tropical forests and rubber plantations in complex landscapes by integrating PALSAR and MODIS imagery. *ISPRS Journal of Photogrammetry and Remote Sensing*, *74*, 20–33.

FAO (2010). *Global forest resources assessment 2010.* (Rome).

Foley, J. A., DeFries, R., Asner, G. P., Barford, C., Bonan, G., Carpenter, S. R., et al. (2005). Global consequences of land use. *Science*, *309*, 570–574.

Foody, G. M. (2010). Assessing the accuracy of land cover change with imperfect ground reference data. *Remote Sensing of Environment*, *114*, 2271–2285.

Fox, J., & Vogler, J. B. (2005). Land-use and land-cover change in montane mainland southeast Asia. *Environmental Management*, *36*, 394–403.

Homer, C., Huang, C. Q., Yang, L. M., Wylie, B., & Coan, M. (2004). Development of a 2001 National Land-Cover Database for the United States. *Photogrammetric Engineering and Remote Sensing*, *70*, 829–840.

Huang, C., Goward, S. N., Masek, J. G., Thomas, N., Zhu, Z., & Vogelmann, J. E. (2010). An automated approach for reconstructing recent forest disturbance history using dense Landsat time series stacks. *Remote Sensing of Environment*, *114*, 183–198.

Huete, A., Didan, K., Miura, T., Rodriguez, E. P., Gao, X., & Ferreira, L. G. (2002). Overview of the radiometric and biophysical performance of the MODIS vegetation indices. *Remote Sensing of Environment*, *83*, 195–213.

Huete, A. R., Liu, H. Q., Batchily, K., & vanLeeuwen, W. (1997). A comparison of vegetation indices over a global set of TM images for EOS-MODIS. *Remote Sensing of Environment*, *59*, 440–451.

Li, Z. (2011). Rubber tree distribution mapping in northeast Thailand. *International Journal of Geosciences*, *02*, 573–584.

Li, H. M., Aide, T. M., Ma, Y. X., Liu, W. J., & Cao, M. (2007). Demand for rubber is causing the loss of high diversity rain forest in SW China. *Biodiversity and Conservation*, *16*, 1731–1745.

Li, Z., & Fox, J. M. (2011). Integrating Mahalanobis typicalities with a neural network for rubber distribution mapping. *Remote Sensing Letters*, *2*, 157–166.

Li, Z., & Fox, J. M. (2012). Mapping rubber tree growth in mainland Southeast Asia using time-series MODIS 250 m NDVI and statistical data. *Applied Geography*, *32*, 420–432.

Longepe, N., Rakwatin, P., Isoguchi, O., Shimada, M., Uryu, Y., & Yulianto, K. (2011). Assessment of ALOS PALSAR 50 m orthorectified FBD data for regional land cover classification by support vector machines. *IEEE Transactions on Geoscience and Remote Sensing*, *49*, 2135–2150.

Masek, J. G., Vermote, E. F., Saleous, N. E., Wolfe, R., Hall, F. G., Huemmrich, K. F., et al. (2006). A Landsat surface reflectance dataset for North America, 1990–2000. *IEEE Geoscience and Remote Sensing Letters*, *3*, 68–72.

Miettinen, J., & Liew, S. C. (2011). Separability of insular Southeast Asian woody plantation species in the 50 m resolution ALOS PALSAR mosaic product. *Remote Sensing Letters*, *2*, 299–307.

Montesano, P. M., Nelson, R., Sun, G., Margolis, H., Kerber, A., & Ranson, K. J. (2009). MODIS tree cover validation for the circumpolar taiga-tundra transition zone. *Remote Sensing of Environment*, *113*, 2130–2141.

NASA Goddard Space Flight Center (2011). Landsat 7 science data users handbook. http://landsathandbook.gsfc.nasa.gov/pdfs/Landsat7_Handbook.pdf

Potere, D. (2008). Horizontal positional accuracy of Google Earth's high-resolution imagery archive. *Sensors*, *8*, 7973–7981.

Qiu, J. (2009). Where the rubber meets the garden. *Nature*, *457*, 246–247.

Richards, J. A., & Jia, X. (1999). *Remote sensing digital image analysis: An introduction* (3rd ed.). Berlin; New York: Springer.

Rosenqvist, A., Shimada, M., Ito, N., & Watanabe, M. (2007). ALOS PALSAR: A Pathfinder mission for global-scale monitoring of the environment. *IEEE Transactions on Geoscience and Remote Sensing*, *45*, 3307–3316.

Santoro, M., Fransson, J. E. S., Eriksson, L. E. B., & Ulander, L. M. H. (2010). Clear-cut detection in Swedish Boreal Forest using multi-temporal ALOS PALSAR backscatter data. *Ieee Journal of Selected Topics in Applied Earth Observations and Remote Sensing*, *3*, 618–631.

Shimada, M., Isoguchi, O., & Rosenqvist, A. (2008). Palsar calval and generation of the continent scale mosaic products for Kyoto and Carbon projects. *Geoscience and remote sensing symposium, 2008. IGARSS 2008. IEEE international* (pp. I-17–I-20).

Shimada, M., & Ohtaki, T. (2010). Generating large-scale high-quality SAR mosaic datasets: Application to PALSAR data for global monitoring. *Ieee Journal of Selected Topics in Applied Earth Observations and Remote Sensing*, *3*, 637–656.

Tan, Z., Yang, X., Ou, Z., Sun, H., Chen, H., & Xi, G. (2010). The extraction of rubber spatial distributing information in hainan province based on FY-3a satellite data. *World Automation Congress (WAC)* (pp. 25–29).

Tucker, C. J. (1979). Red and photographic infrared linear combinations for monitoring vegetation. *Remote Sensing of Environment*, *8*, 127–150.

Vermote, E. F., ElSaleous, N., Justice, C. O., Kaufman, Y. J., Privette, J. L., Remer, L., et al. (1997). Atmospheric correction of visible to middle-infrared EOS-MODIS data over land surfaces: Background, operational algorithm and validation. *Journal of Geophysical Research-Atmospheres*, *102*, 17131–17141.

Walker, W. S., Stickler, C. M., Kellndorfer, J. M., Kirsch, K. M., & Nepstad, D. C. (2010). Large-area classification and mapping of forest and land cover in the Brazilian Amazon: A comparative analysis of alos/palsar and landsat data sources. *Ieee Journal of Selected Topics in Applied Earth Observations and Remote Sensing*, *3*, 594–604.

Wu, F., Wang, C., Zhang, H., Zhang, B., & Tang, Y. X. (2011). Rice crop monitoring in South China with RADARSAT-2 quad-polarization SAR data. *IEEE Geoscience and Remote Sensing Letters*, *8*, 196–200.

Xiao, X., Biradar, C., Czarnecki, C., Alabi, T., & Keller, M. (2009). A simple algorithm for large-scale mapping of evergreen forests in tropical America, Africa and Asia. *Remote Sensing*, *1*, 355–374.

Xiao, X., Dorovskoy, P., Biradar, C., & Bridge, E. (2011). A library of georeferenced photos from the field. *EOS Transactions of the American Geophysical Union*, *92*.

Xiao, X. M., Hollinger, D., Aber, J., Goltz, M., Davidson, E. A., Zhang, Q. Y., et al. (2004). Satellite-based modeling of gross primary production in an evergreen needleleaf forest. *Remote Sensing of Environment*, *89*, 519–534.

Xiao, W., Wang, X., & Ling, F. (2010). The application of ALOS PALSAR data on mangrove forest extraction. *Remote Sensing Technology and Application*, *25*, 91–96.

Xiao, X. M., Zhang, Q. Y., Hollinger, D., Aber, J., & Moore, B. (2005). Modeling gross primary production of an evergreen needleleaf forest using modis and climate data. *Ecological Applications*, *15*, 954–969.

Xu, N. (2010). Why the average yield of private rubber plantations more than state farms in Hainan. *Chinese Journal of Tropical Agriculture*, *30*, 56–60.

Zhai, D. L., Cannon, C. H., Slik, J. W. F., Zhang, C. P., & Dai, Z. C. (2012). Rubber and pulp plantations represent a double threat to Hainan's natural tropical forests. *Journal of Environmental Management*, *96*, 64–73.

Zhang, J., Tao, Z., Liu, S., Cai, D., Tian, G., Xie, R., et al. (2010). Rubber planting acreage calculation in Hainan Island based on TM image. *Chinese journal of tropical crops*, *31*, 661–665.

Ziegler, A. D., Fox, J. M., & Xu, J. C. (2009). The rubber juggernaut. *Science*, *324*, 1024–1025.